How to cite: *Angew. Chem. Int. Ed.* **2024**, *63*, e202403790
doi.org/10.1002/anie.202403790

Explosive Emulsification

Oversaturating Liquid Interfaces with Nanoparticle-Surfactants

*Xuefei Wu[+], Han Xue[+], Zachary Fink, Brett A. Helms, Paul D. Ashby, Ahmad K. Omar, and Thomas P. Russell**

Abstract: Assemblies of nanoparticles at liquid interfaces hold promise as dynamic "active" systems when there are convenient methods to drive the system out of equilibrium via crowding. To this end, we show that oversaturated assemblies of charged nanoparticles can be realized and held in that state with an external electric field. Upon removal of the field, strong interparticle repulsive forces cause a high in-plane electrostatic pressure that is released in an explosive emulsification. We quantify the packing of the assembly as it is driven into the oversaturated state under an applied electric field. Physiochemical conditions substantially affect the intensity of the induced explosive emulsification, underscoring the crucial role of interparticle electrostatic repulsion.

Introduction

Out-of-equilibrium self-assembled structures underpin many "active" systems that mimic living systems.[1] Many intricate structures and functions within living organisms are a result of non-equilibrium assemblies on length scales ranging from the molecular to cellular levels.[2] However, unlike self-assembled systems at equilibrium, where thermodynamic variables dictate the packing and saturation conditions, out-of-equilibrium assemblies can be kinetically trapped in states or structures well-below or well-above the equilibrium saturation point.

Out-of-equilibrium self-assembled structures can be generated through the use of an external field. The field may be in the form of a time-varying temperature, or the use of an applied field, e.g., an electric[3]/magnetic[4] field, light,[1c,5] chemical fuel,[6] or fluid flow,[7] that forces a non-equilibrium packing of the assembly. Depending on the components comprising the assembly, the spatial arrangements of the components in the non-equilibrium assembly can impart properties or functions far different from the assembly at equilibrium. Subsequent to the removal of the field, the system attempts to relax to the equilibrium state, but how rapidly this relaxation occurs will be system- and condition-dependent. If non-equilibrium assemblies are vitrified or jammed,[8] relaxation is markedly slowed or arrested. If non-equilibrium assemblies are ordered or there are strong interparticle interactions,[1c] relaxations can also be exceedingly slow.

To realize the out-of-equilibrium assemblies at the interface, one needs to first to control the adsorption of nanoparticles (NPs) to the liquid/liquid interface and prevent aggregation-induced irreversible close packing. Diffusion-driven[9] and ethanol-induced[10] adsorption to the liquid interface are among the most widely used strategies. Spontaneous self-assembly is the most convenient method, however, this approach has often led to inhomogeneous packing of the NPs, as well as, the appearance of areas with low area coverage.[9] Here, we exploit the electrostatic interactions between the charged NPs dispersed in the aqueous phase and surfactants dissolved in the oil phase, along with complementary counterions forming the nanoparticle-surfactants (NPSs)[8] that can generate a densely packed 2D film at the liquid/liquid interface.[11] This allows for the adjustment of interparticle interactions by modulating the electrostatic forces between the particles by the addition of electrolytes,[12] pH adjustments,[13] or concentration changes.[14] This method affords a simple route to achieve densely packed NPs assemblies at the liquid/liquid interface and does not depend on the incorporation of lower-dielectric constant solvents. Therefore, in this manu-

[*] Dr. X. Wu,[+] Dr. H. Xue,[+] Dr. Z. Fink, Dr. B. A. Helms, Prof. A. K. Omar, Prof. T. P. Russell
Materials Sciences Division
Lawrence Berkeley National Laboratory
Berkeley, CA-94720, USA
E-mail: russell@mail.pse.umass.edu

Dr. Z. Fink, Prof. T. P. Russell
Polymer Science and Engineering Department
University of Massachusetts
Amherst, MA-01003, USA

Dr. B. A. Helms, Dr. P. D. Ashby
Molecular Foundry
Lawrence Berkeley National Laboratory
Berkeley, CA-94720, USA

Prof. A. K. Omar
Department of Materials Science and Engineering
University of California, Berkeley
Berkeley, CA-94720, USA

Prof. T. P. Russell
Advanced Institute for Materials Research (AIMR)
Tohoku University
2-1-1 Katahira, Aoba, Sendai 980-8577, Japan

[+] These authors contributed to this work equally.

script, we used this method to facilitate the spontaneous adsorption of NPs at a water/oil interface.

When NPs are oversaturated at an interface due to the application of an external field, their stability post-field removal is influenced by their binding energy to the interface and their interactions with each other. Usually, NPs have a low binding energy, leading to their ejection from the interface to alleviate stress.[15] Previous studies have shown that voltage-tunable charged NPs arrays at liquid/liquid interfaces can produce electro-tunable quasi-two-dimensional plasmonic platforms by adjusting the packing densities at the interfaces.[15–16] The application of an electric field can either drive these charged NPs toward or away from the interface, depending on the direction of the applied field. At the interface, a potential energy well causes the NPs to overcome the electrostatic repulsion between the NPs, thereby increasing their reversible packing density. However, by attaching ligands to form NPSs, this binding energy increases, preventing ejection and arresting the system in a jammed non-equilibrium state.[8,17] If the NPSs are charged, the strong interparticle electrostatic repulsion leads to explosive emulsification after rapid field removal.[18] Here, the rapid ejection of hundreds of thousands of charged microdroplets decorated with a jammed layer of NPSs, forms a charged plume that propels the parent droplet by electrostatic forces, turning it into an "active droplet".[19]

To better understand the behavior of NPS assemblies, it is important to link their macroscopic behavior to nanoscopic structure. Due to the small size of NPs, the available experimental techniques for in situ investigation of assemblies at liquid/liquid interfaces are limited. Liquid cell transmission electron microscopy offers one method, but it is hindered by the requirement of thin liquid layers and difficulties in applying a field.[20] Open cell scanning electron microscopy can detail NP or NPS assemblies on a surface, but cannot easily access a liquid/liquid interface.[21] Surface Enhanced Raman scattering (SERS) of molecules near the gold NPs (Au NPs) allows for the detection and identification of molecular species at very low concentrations,[22] but it can only detect a target with a Raman signal.[23] UV/Vis measurements can extract NP spatial information through localized plasmon coupling between the NPs, yet its sensitivity diminishes at greater interparticle distances.[24] In situ grazing incidence small-angle X-ray scattering, however, is ideally suited to characterize the in-plane and out-of-plane packing of NPS assembled at a fluid/fluid interface.[11,25]

Here, in situ X-ray scattering is used to elucidate the NPS packing microstructure at a water/toluene interface under an applied electric field in real time (Figure 1a). The distance between NPSs is found to decrease with external electric field intensity as the NPS packing densifies until oversaturation. The balance between electrostatic repulsion between NPSs at the interface and their response to the applied field determines the level of oversaturation and the intensity of the explosive emulsification realized after field removal. Increasing ligand concentration intensifies this emulsification, especially under alkaline conditions. However, if ligand concentration surpasses a threshold, oversaturation of the NPSs cannot be achieved and only spontaneous emulsification is found.

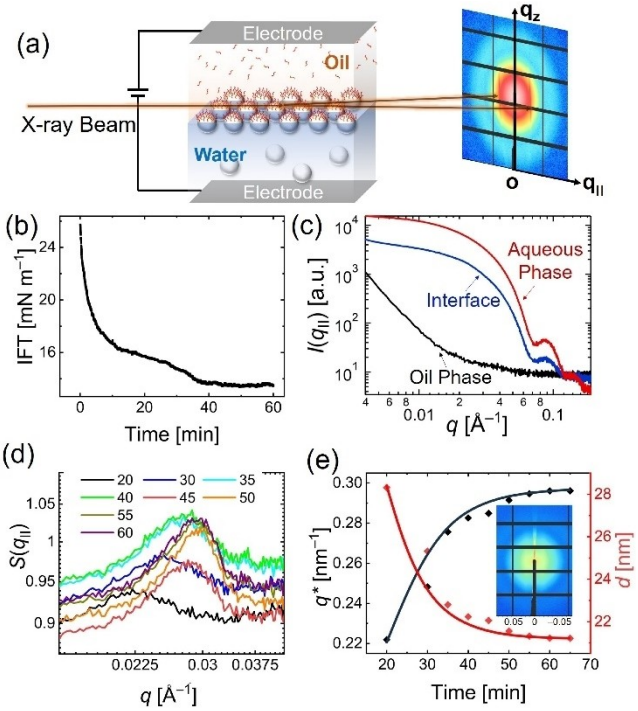

Figure 1. (a) In situ X-ray scattering experiments on NPS assemblies at the water/oil bilayer interface while subjected to an external electric field. (b) Interfacial tension IFT vs interface aging time measured by the pendant drop tensiometer under no field. The concentration of Au NPs is 3.6 nM and that of the PS-triNH$_2$ is 1 mg mL^{-1}. (c) 1D X-ray scattering spectra, $I(q_{||})$, of bulk oil (black), bulk Au NPs phase (red) and interfacial region (blue) of a water/toluene bilayer. (d) Time evolution of the structure factor, $S(q_{||})$, of Au NPSs monolayer at the interface at different aging times without an electric field. Time in minutes is indicated in the legend. (e) The relationship between the mean peak position, q^*, and center-to-center interparticle distance, d, between the NPSs with time. The inset shows the 2D X-ray scattering signal obtained from an interface laden with Au NPs after aging for 20 min.

Results and Discussion

Figure 1a shows the in situ X-ray scattering measurements on a dense assembly of spherical Au NPs at the interface of a water/toluene bilayer with/without an external electric field. A planar interface is prepared between an aqueous dispersion of carboxyl-functionalized Au NPs and a toluene solution of ω-(diethylene triamine)-terminated polystyrene (PS-triNH$_2$) that is used to facilitate the adsorption of the NPs to the interface. PS-triNH$_2$ has pKa values at ~4, 7.5, and 10, due to its triamine structure, and the carboxylic acid-functionalized Au NPs has a pKa value at ~5. At a neutral pH of 7, the majority of the carboxylic acids on the surface of the NPs are deprotonated, causing the NPs to be highly negatively charged (Figure S1). Surfactant molecules spontaneously adsorb to the interface to reduce the interfacial

tension (IFT) (Figure S2), which increases as the pH increases due to the reduced protonation at higher pH levels. Concurrently, the amine groups within the ligand become protonated upon contact with the interface, resulting in a positive charge. The strong electrostatic interactions between the negatively charged Au NPs and the cationic surfactant, PS-triNH_2, leads to a substantial enhancement in the binding energy per NP by anchoring the absorbed ligands at the interface to the NPs, which facilitates the densification of the assembly and reduces the IFT substantially (Figure 1b and Figures S2–S3). All the IFT data given in this manuscript were measured with a pendant drop tensiometer.

Absent an external field, it is observed that the IFT of the interface decorated with NPSs is gradually decreased with time, and the change in the IFT should be directly related to the packing density of the NPSs at the interface. The IFT initially shows a rapid decrease (<12 min), as the NPSs form and assemble at the interface. It then shows a more gradual decrease (12–28 min), as more NPSs form and assemble at the interface, where the amount of space remaining at the interface is reduced and the adsorption is slowed. Further reorganization of the NPSs at the interface due to interparticle interactions, e.g., capillary forces,[26] that densifies the assembly further gives rise to the step decrease in the IFT (~30 min), after which the IFT plateaus at a value of ~13.5 mN m^{-1}. The balance between electrostatic repulsion and capillary attraction among the NPSs establishes the equilibrium distance between particles.

During the in situ scattering measurement, as the X-ray beam is scanned vertically from the toluene to water phases, the interface is located from a sharp decrease in the transmitted intensity. We note that the scattering experiments were not performed on a pendant drop, due to the absorption of the X-rays, but at the interface between an oil/water bilayer. Attempts were made to replicate the conditions of the pendant drop studies as precisely as possible. The Au NPs dispersed in the aqueous phase are first characterized by X-ray scattering, as shown in Figure S4. The dispersion of NPs in the aqueous phase shows a series of maxima as a function of the scattering vector,

$$q = \left(\frac{4\pi}{\lambda}\right)\sin\theta$$

where 2θ is the scattering angle and λ is the wavelength, characteristic of the sphere scattering function, while the scattering from the toluene solution of the PS-triNH_2 ligands monotonically decreases as a function of q, as would be expected. The scattering from the interfacial region, while closely resembling the scattering from the aqueous dispersion of NPs, shows some distinct differences (Figure 1c). Here, the incident X-ray beam, ~0.5 mm in diameter, intercepts not only the assembly of NPs at the interface, but also the liquid phases above and below the interface. Even though the thickness of the NPSs assembly is small in comparison to the beam diameter, the areal density of the NPSs is orders of magnitude higher than the number of NPs in the dispersion intercepted by the beam (Figure S5). The in-plane scattering, $I(q)$, can reasonably be treated as the product of the form factor $P(q)$, characteristic of the NP size and shape, and structure factor $S(q)$, characteristic of the in-plane packing of the NPSs. The scattering from NP dispersion in the aqueous phase gives $P(q)$. Therefore, the structure factor of the NPS assembly at the interface can be well approximated by[27]

$$S(q) = \frac{I(q)}{P(q)}$$

$S(q)$ for the in-plane scattering of the assembly of NPSs at the interface is shown in Figure 1d as a function of time. A distinct maximum in $S(q)$ is evident, characteristic of the average center-to-center distance, d, between the NPSs. The peak position, q^*, shifts to higher q over time, corresponding to a decrease in the center-to-center distance from 28.3 nm to 21.5 nm, as shown in Figure 1e. The progressive increase in the integrated area and decrease in the full width at half maximum under the interference maximum signify an increase in the number of NPS assembled at the interface and an enhancement in the in-plane correlations within the self-assembled NPS array (Figure S6). After the formation and assembly of the NPSs at the interface, scattering rods are evident, characteristic of an Au NPS monolayer at the interface (inset in Figure 1e). The broad size distribution of the NPs prevents the long–range structural ordering of the interfacial assembly even at high areal densities (Figure S7). A plot of the IFT and NP interparticle distance as a function time clearly shows the close correlation between the two (Figure S8).

The application of an electric field enables the manipulation of the packing of the NPSs at the interface, leading to an oversaturated assembly. With a negatively polarized aqueous phase, the NPs are stable at the interface until the voltage is turned off, whereupon a burst of microdroplets are explosively ejected from the interface (Figures 2a–b and Movie S1). Irregular shaped microdroplets, e.g., cylindrical, triangular, and ellipsoidal, are seen optical microscopically (Figure S9), indicating that NPS assemblies on the microdroplet surfaces are jammed, preventing them from relaxing to a spherical shape.[8a,28] The number and speed of the jettisoned microdroplets increase with increasing applied voltage, due to the oversaturation of the NPSs at the interface driven by the negative potential drop across the interface. This phenomenon was previously analyzed through IFT data to indirectly infer the packing density,[19] while we're trying to quantitively characterize this behavior here.

In situ small angle X-ray scattering is used to investigate the packing of the NPSs at the water/toluene bilayer interface under an applied electric field, as shown in Figure 1a. When subjected to an external electric field (with the aqueous phase negatively polarized), cations that reside in the aqueous phase are moved away from the interface while the negative ions and NPs are forced towards the interface, leading an increased electrostatic repulsion between the NPSs at the interface. The external field can overcome this repulsion, thereby increasing the areal density

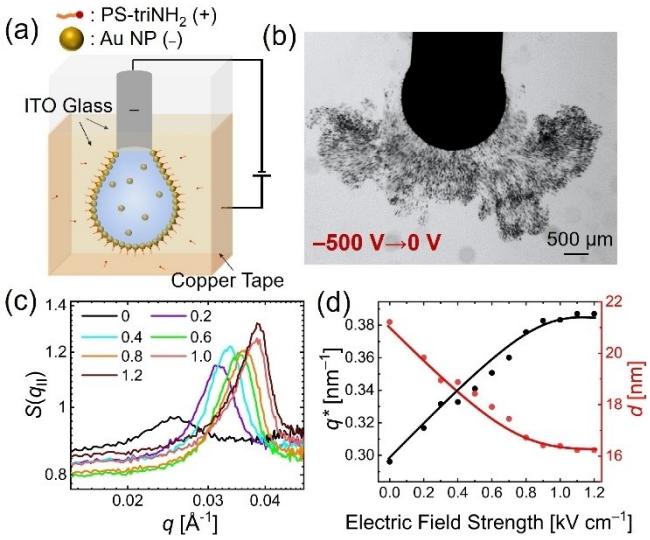

Figure 2. (a) Schematic of the pendant droplet explosive emulsification experimental setup. A pendant aqueous droplet is immersed in the toluene phase and hung at the end of a stainless-steel needle enabling application of a negative bias voltage. The conductive chamber holding the polystyrene solution acts as the counter electrode. (b) The optical image of the aqueous droplet ($C_{Au}=3.6$ nM) immersed in a PS-triNH$_2$ solution (1 mg mL^{-1}) in toluene when a bias voltage of −500 V applied to the needle is turned off. (c) Structure factor, $S(q_{II})$, of the bilayer interface packed Au NPSs monolayer, dependent on the external applied field. The electric field strength in kV cm^{-1} is indicated in legend. (d) The relationship between q^* and d with the applied electric field strength.

of NPSs at the interface. The water/toluene interface, on the other hand, becomes increasingly more negatively charged, inhibiting the further approach of negatively charged NPs, once the repulsion between the negatively charged interface and the NPs becomes stronger than or equal to the force exerted by the external field (Figure S5). We note that an applied field also enhances the transport of uncharged PS-triNH$_2$ to the interface, due to electrohydrodynamic flows generated on both sides of the interface.[29] Although the capillary tube and the pendant droplet show different meniscus formations, the particles involved are comparatively much smaller, and the effect of curvature can be ignored in the data analysis. As the applied external field is increased in a stepwise manner, the position of the interference maximum shifts to higher q (Figures 2c–d), showing that the areal density of NPSs at the interface increases. Since the interfacial area has not changed, this result also indicates that the number of NPSs at the interface has increased. Absent an external field, the equilibrium interparticle distance is ~21.5 nm (Figure 1), ~40 % of 2D areal fraction. The high degree of deprotonation of the carboxyl ion groups at a neutral pH enhances the interparticle electrostatic repulsion and inhibits a denser packing of the NPSs (Figure 1 and Figure S1). However, when an electric field is applied, NPS areal density significantly increases, overcoming the interparticle repulsion, up to several tens of nN,[30] and reducing the distance between them to 16.2 nm (71 %), nearly the size of a single particle (Figure 2), which results in the accumulation of Coulombic energy within the oversaturated assemblies and rapid dissipation of the energy after removal of external field. From the 2D scattering image, Bragg rods, interference maxima extended normal to the plane of the interface, are clearly evident, which are characteristic of the monolayer nature of the NPS assembly. Although the electric field depletes the free cations at the interface and enhances the interparticle electrostatic repulsion, the external electric field is sufficiently strong to overcome these and densify the NPS packing. It's worth highlighting that the electric field strength has a significant impact on the oversaturation extent of NPS assemblies at the interface. Notably, the q^* position remains stable even after a prolonged aging period (Figure S10), but it clearly shifts to a higher q position under the influence of a stronger electric field. The increase in integrated peak area with increasing applied electric field also clearly reflects the increase in the number of NPSs that are strongly bound to the interface[16b] (Figure S11). With the anchoring of the cationic surfactants to the Au NPs, the binding energy per particle at the interface is significantly increased, suppressing any desorption of the individual NPs from the interface. However, when the field is turned off, the in-plane pressure arising from the electrostatic repulsion between the NPSs destabilizes the interface and triggers an explosive emulsification with hundreds of thousands of microdroplets coated with a monolayer of NPSs being jettisoned from the interface into the oil phase (Figure 2b). Notably, reversing the field direction, with a positively charged needle, does not result in this behavior and barely affects X-ray scattering, showing no additional Au NPs are drawn to the interface (Figure S12).

The degree of deprotonation of the carboxyl groups, which influences the interparticle electrostatic interactions, also alters the ability of the NPSs assemblies to store the potential energy at the interface, and depends on the pH of the aqueous phase. At lower pH values, most of the amine groups of the ligands adsorbed at the interface become protonated, increasing their interfacial activity (Figure S2) and strong affinity to the negatively charged NPs. However, for the carboxylic acid-functionalized NPs, fewer carboxyl groups are deprotonated, resulting in a lower charge density (Figure S1). This, in turn, considerably diminishes the electrostatic repulsion between particles, and reduces the equilibrium interparticle distance. Absent an external field, at pH of 4, the equilibrium center-to-center distance is ~17 nm, reducing the IFT to ~12.1 mN m^{-1} (Figures 3a–b). This can be attributed to the weak electrostatic repulsion between neighboring Au NPs and the strong interfacial activity of the polystyrene surfactants that strongly anchor the NPSs to the interface. The application of an electric field only marginally enhances the packing density of the Au NPs due to their inherent tightly-packed structure. This is evident from the shift of the scattering peak to higher q values, ranging from 0.363 nm^{-1} to 0.388 nm^{-1}, with the interparticle distance decreasing from 17.3 nm to 16.2 nm (Figure S13). The narrowing of the Bragg peak also suggests enhanced nanoparticle correlations at the interface. However, the weak electrostatic repulsion between the Au NPSs reduces

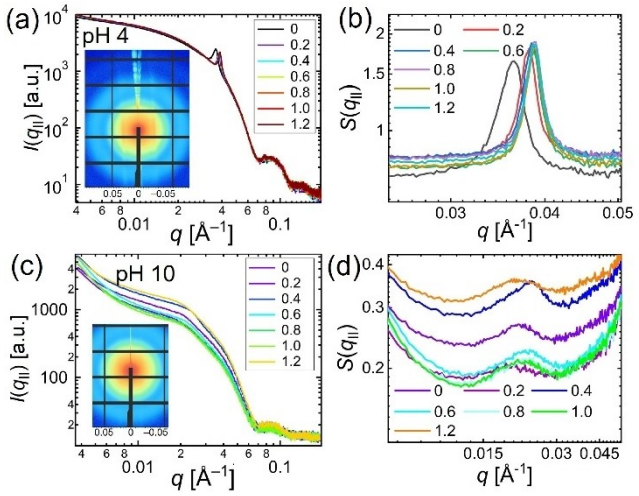

Figure 3. (a) 1D scattering profile, $I(q_{II})$ and, (b) structure factor, $S(q_{II})$, of the NP-laden interface between water/toluene bilayer at pH of 4 varying with the electric field strength. (c) $I(q_{II})$, and (d) $S(q_{II})$, of the NP-laden interface between water/toluene bilayer and at pH of 10 varying with the electric field strength. The insets in (a) and (c) display the 2D X-ray scattering signal of the interface under pH of 4 and 10, respectively. The electric field strength in kV cm^{-1} is indicated in all the legends.

the accumulated electrostatic energy at maximum packing, weakening the explosive emulsification behavior.

Under alkaline conditions (Figures 3c–d), PS-triNH$_2$ maintains its interfacial activity, though the electrostatic attraction between the ligand and NPs diminishes as the amine groups become less protonated. Consequently, the areal density of Au NPSs assembled at the interface is much lower, with an average interparticle distance of ~30 nm, corresponding to a higher IFT of 15.3 mN m^{-1}. In addition to the charge density of the NPs, the interfacial activity of the polymer surfactant plays an important role in generating the out-of-equilibrium system. The adsorption and protonation of cationic surfactants decrease with increasing pH. Consequently, absent electrostatic attractions from the surfactants at the interface, the negatively charged Au NPs tend to remain dispersed in the bulk phase rather than adsorbing at the interface due to the inherently negatively charged water/oil interface.[31] Upon applying the electric field, a noticeable shift in the peak position is observed in the X-ray scattering profiles. At low electric field strength (<0.8 kV cm^{-1}), the peak position moves towards higher q values, and at high electric field strength (>0.8 kV cm^{-1}), the interparticle repulsion becomes stronger due to the depletion of the counterions from the interface,[25d] which drives the q back to lower values. This non-monotonic behavior is not observed under neutral/acid conditions, due to the higher interfacial activity of the cationic ligands that anchor to the interface through stronger protonation of the amine groups. To be noted that even with a medium electric field (0.4–1.0 kV cm^{-1}), the Au NPs still remain dispersed with relatively large interparticle distances for those NPSs formed at the interface, ~27 nm, that minimizes the interparticle interactions. As a result, while the high degree of deprotonation of the carboxyl group does enhance the charge density of each NP in an alkaline solution, the large interparticle distances for those NPSs formed at the interface reduces the interparticle interactions even under the field (Figure S13), weakening the explosive behavior.

At high ligand concentration, well above the critical micelle concentration, spontaneous emulsification occurs, limiting the areal density of the Au NPs at the interface. Spontaneous emulsification begins at ~10.5 mN m^{-1}, after an aging time of 30 s (Figure 4a). Consequently, while the adsorption of the cationic ligand weakens the electrostatic repulsion, the interparticle distance is limited to 21.8 nm due to the spontaneous emulsification (Figure 4b). Under the influence of the electric field, a shift towards higher q values is still observed, reducing the interparticle distance to 20.8 nm, which is a curious result due to the fact that both the number of NPs and also the area of the parent droplet are decreasing during spontaneous emulsification (Figure S14).

As previously mentioned, the efficient generation of an out-of-equilibrium system depends on the physiochemical conditions, such as pH and component concentrations. We quantified the intensity of explosive emulsification formed at different pH and ligand concentrations (Figure 4c). The largest number of microdroplets jettisoned from the interface during explosive emulsification occurs at pH 10 and a

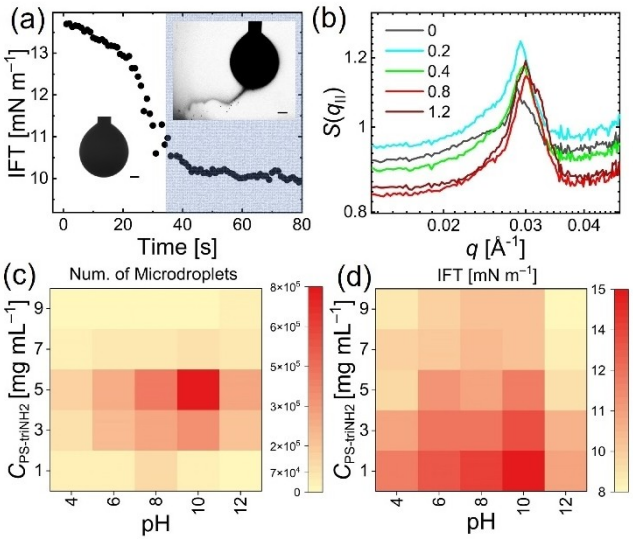

Figure 4. (a) Time evolution of the IFT at high ligand concentration of 10 mg mL^{-1} measured by the pendant drop tensiometer. The inset image at the clear area displays the optical image of the pendant aqueous droplet immediately after immersion into the toluene phase, and that at the grid-like blue area reveals the droplet undergoing spontaneous emulsification. Scale bar: 500 μm. (b) $S(q_{II})$ of the NP-laden interface between water/toluene bilayer, dependence on the external applied field, at pH 7 and a ligand concentration of 10 mg mL^{-1}. The electric field strength in kV cm^{-1} is indicated in the legend. (c) The dependence of the total number of the microdroplets jettisoned from a pendant droplet during the explosive emulsification on both pH and ligand concentration. (d) The dependence of the IFT value on both pH and ligand concentration measured by the pendant drop tensiometer.

ligand concentration of 5 mg mL^{-1}. However, as the ligand concentration is decreased below this, the pH associated with the maximum microdroplet formation gradually shifts towards neutral conditions. Thus, explosive emulsification depends on the interplay between interparticle interactions and the areal density. As the ligand concentration increases, more Au NPs adsorb to the interface, and form NPSs. This interaction weakens the electrostatic repulsion, leading to a weakening of the explosive behavior. To compensate, the pH must be increased to mitigate the adsorption of the ligands, thereby enhancing interparticle repulsion. By doing so, the system is tuned to promote explosive emulsification.

Based on the IFT data (Figure 4d), a very low IFT is not required to induce out-of-equilibrium behavior. On the contrary, the most intense explosive emulsification at each concentration typically takes place at relatively high IFTs, since the interface can accommodate a larger number of the excess NPs from the bulk phase and store more potential energy. It is important, though, that the Au NPSs not be too far apart to enhance the interparticle interactions. Titration studies indicate that each individual NP bears ~200 carboxyl groups. Consequently, even a minor reduction in the interparticle distance, for example, from 22 nm to 17 nm, can cause the potential energy to increase by 10^{-5} J, sufficient to offset the energy needed to expand the interface and to propel the microdroplets away from the interface at high speeds. Nevertheless, beyond a concentration of 5 mg mL^{-1}, spontaneous emulsification occurs, due to micelle solubilization.[32] This leads to a weakening of the explosive emulsification and prevents any further decrease in IFT with increasing ligand concentration.

Conclusion

Collectively, we conclude that by adopting X-ray scattering method, in situ characterization of interfacial assembly microstructure with and without an applied field is realized quantitatively, and further, our results indicate that the electric field can store Coulombic energy at immiscible liquid/liquid interfaces by oversaturating the packing of charged NPSs. Physicochemical conditions, e.g., pH and ligand concentration, can modify the binding energy of NPSs to the interface, markedly influencing the explosive behavior. Higher ligand concentrations enhance explosive emulsification under alkaline conditions more significantly, but beyond a threshold concentration, spontaneous emulsification dominates, limiting NPSs densification under the field. This research highlights the intricate balance of factors that influence out-of-equilibrium assemblies at interfaces, and also emphasizes the importance of tailoring physicochemical conditions to achieve precise control over explosive emulsification behavior, which guides further research towards achieving controllable explosive emulsification and designing an active droplet system tailored to specific needs. The explosive emulsification behavior shows that the liquid/liquid interface acts as a dynamic reservoir, storing energy by accumulating an oversaturated layer of charged NPSs, underscoring its potential for applications in self-propulsion systems and remotely operated soft microrobots.

Supporting Information

The authors have cited additional references within the Supporting Information.[33]

Acknowledgements

This work was supported by the U.S. Department of Energy, Office of Science, Office of Basic Energy Sciences, Materials Sciences and Engineering Division under Contract No. DE-AC02-05-CH11231 within the Adaptive Interfacial Assemblies Towards Structuring Liquids program (KCTR16). Beamline 7.3.3 of the Advanced Light Source is supported by the Director of the Office of Science, Office of Basic Energy Sciences, of the U.S. Department of Energy under Contract No. DE-AC02-05CH11231.

Conflict of Interest

The authors declare no conflict of interest.

Data Availability Statement

The data that support the findings of this study are available from the corresponding author upon reasonable request.

Keywords: out-of-equilibrium assembly · nanoparticle-surfactants · in situ small-angle X-ray scattering · explosive emulsification · liquid/liquid interface

[1] a) B. A. Grzybowski, K. Fitzner, J. Paczesny, S. Granick, *Chem. Soc. Rev.* **2017**, *46*, 5647; b) D. Babu, N. Katsonis, F. Lancia, R. Plamont, A. Ryabchun, *Nat. Chem. Rev.* **2022**, *6*, 377; c) R. Klajn, K. J. Bishop, B. A. Grzybowski, *Proc. Natl. Acad. Sci. USA* **2007**, *104*, 10305; d) R. M. Erb, H. S. Son, B. Samanta, V. M. Rotello, B. B. Yellen, *Nature* **2009**, *457*, 999.

[2] a) G. M. Whitesides, B. Grzybowski, *Science* **2002**, *295*, 2418; b) X. Fang, K. Kruse, T. Lu, J. Wang, *Rev. Mod. Phys.* **2019**, *91*, 045004; c) T. D. Pollard, G. G. Borisy, *Cell* **2003**, *112*, 453.

[3] a) M. Li, D. Li, *J. Nanopart. Res.* **2016**, *18*, 120; b) B. Bharti, O. D. Velev, *Langmuir* **2015**, *31*, 7897; c) A. A. Harraq, B. D. Choudhury, B. Bharti, *Langmuir* **2022**, *38*, 3001; d) P. Dommersnes, Z. Rozynek, A. Mikkelsen, R. Castberg, K. Kjerstad, K. Hersvik, J. Otto Fossum, *Nat. Commun.* **2013**, *4*, 2066.

[4] a) A. Snezhko, I. S. Aranson, *Nat. Mater.* **2011**, *10*, 698; b) G. Kokot, D. Piet, M. Whitesides, I. S. Aranson, A. Snezhko, *Sci. Rep.* **2015**, *5*, 9528; c) J. L. Aragones, J. P. Steimel, A. Alexander-Katz, *Soft Matter* **2019**, *15*, 3929.

[5] a) D. Manna, T. Udayabhaskararao, H. Zhao, R. Klajn, *Angew. Chem. Int. Ed. Engl.* **2015**, *54*, 12394; b) J. W. Lee, R. Klajn, *Chem. Commun.* **2015**, *51*, 2036.

[6] W. Wang, W. Duan, A. Sen, T. E. Mallouk, *Proc. Natl. Acad. Sci. USA* **2013**, *110*, 17744.

[7] a) W. Lee, H. Amini, H. A. Stone, *Proc. Natl. Acad. Sci. USA* **2010**, *107*, 22413; b) H. Song, D. L. Chen, R. F. Ismagilov, *Angew. Chem. Int. Ed. Engl.* **2006**, *45*, 7336; c) A. S. Utada, E. Lorenceau, D. R. Link, P. D. Kaplan, H. A. Stone, D. A. Weitz, *Science* **2005**, *308*, 537.
[8] a) M. Cui, T. Emrick, T. P. Russell, *Science* **2013**, *25*, 460; b) X. Liu, N. Kent, A. Ceballos, R. Streubel, Y. Jiang, Y. Chai, P. Y. Kim, J. Forth, F. Hellman, S. Shi, D. Wang, B. A. Helms, P. D. Ashby, P. Fischer, T. P. Russell, *Science* **2019**, *365*, 264.
[9] Y. Zou, Z. Wan, J. Guo, J. Wang, S. Yin, X. Yang, *Food Hydrocolloids* **2017**, *63*, 364.
[10] a) Y.-K. Park, S.-H. Yoo, S. Park, *Langmuir* **2007**, *23*, 10505; b) H. Jia, Y. F. Zhang, C. Zhang, M. Ouyang, S. Du, *Phys. Chem. B* **2023**, *127*, 2258; c) L. Song, B. B. Xu, Q. Cheng, X. Wang, X. Luo, X. Chen, T. Chen, Y. Huang, *Sci. Adv.* **2021**, *7*, eabk2852.
[11] P. Y. Kim, Z. Fink, Q. Zhang, E. M. Dufresne, S. Narayanan, T. P. Russell, *ACS Nano* **2022**, *16*, 8967.
[12] Y. Chai, A. Lukito, Y. Jiang, P. D. Ashby, T. P. Russell, *Nano Lett.* **2017**, *17*, 6453.
[13] a) C. Huang, Z. Sun, M. Cui, F. Liu, B. A. Helms, T. P. Russell, *Adv. Mater.* **2016**, *28*, 6612; b) R. Xu, T. Liu, H. Sun, B. Wang, S. Shi, T. P. Russell, *ACS Appl. Mater. Interfaces* **2020**, *12*, 18116.
[14] B. Qian, S. Shi, H. Wang, T. P. Russell, *ACS Appl. Mater. Interfaces* **2020**, *12*, 13551.
[15] B. Su, J.-P. Abid, D. J. Fermin, H. H. Girault, H. Hoffmannova, P. Krtil, Z. Samec, *J. Am. Chem. Soc.* **2004**, *126*, 915.
[16] a) Y. Montelongo, D. Sikdar, Y. Ma, A. J. S. McIntosh, L. Velleman, A. R. Kucernak, J. B. Edel, A. A. Kornyshev, *Nat. Mater.* **2017**, *16*, 1127; b) M. E. Flatté, A. A. Kornyshev, M. Urbakh, *J. Phys. Condens. Matter* **2008**, *20*, 073102.
[17] A. Boker, J. He, T. Emrick, T. P. Russell, *Soft Matter* **2007**, *3*, 1231.
[18] X. Wu, G. Bordia, R. Streubel, J. Hasnain, C. C. S. Pedroso, B. E. Cohen, B. Rad, P. Ashby, A. K. Omar, P. L. Geissler, D. Wang, H. Xue, J. Wang, T. P. Russell, *Adv. Funct. Mater.* **2023**, *33*, 2213844.
[19] X. Wu, H. Xue, G. Bordia, Z. Fink, P. Y. Kim, R. Streubel, J. Han, B. A. Helms, P. Ashby, A. K. Omar, T. P. Russell, *Adv. Mater.* **2024**, 2310435.
[20] R. Yang, L. Mei, Y. Fan, Q. Zhang, H. G. Liao, J. Yang, J. Li, Z. Zeng, *Nat. Protoc.* **2023**, *18*, 555.
[21] a) P. Y. Kim, Y. Gao, Y. Chai, P. D. Ashby, A. E. Ribbe, D. A. Hoagland, T. P. Russell, *ACS Nano* **2019**, *13*, 3075; b) P. Y. Kim, Y. Gao, Z. Fink, A. E. Ribbe, D. A. Hoagland, T. P. Russell, *ACS Nano* **2022**, *16*, 5496.
[22] a) P. Pienpinijtham, X. X. Han, S. Ekgasit, Y. Ozaki, *Phys. Chem. Chem. Phys.* **2012**, *14*, 10132; b) M. P. Cecchini, V. A. Turek, A. Demetriadou, G. Britovsek, T. Welton, A. A. Kornyshev, J. D. E. T. Wilton-Ely, J. B. Edel, *Adv. Opt. Mater.* **2014**, *2*, 966.
[23] a) H. Tian, H. Li, Y. Fang, *ACS Appl. Mater. Interfaces* **2019**, *11*, 16207; b) K. Bramhaiah, N. S. John, *RSC Adv.* **2013**, *3*, 7765; c) K. Kim, H. S. Han, I. Choi, C. Lee, S. Hong, S. H. Suh, L. P. Lee, T. Kang, *Nat. Commun.* **2013**, *4*, 2182.
[24] a) P. K. Jain, W. Huang, M. A. El-Sayed, *Nano Lett.* **2007**, *7*, 2080; b) V. A. Turek, M. P. Cecchini, J. Paget, A. R. Kucernak, A. A. Kornyshev, J. B. Edel, *ACS Nano* **2012**, *6*, 7789; c) Z. Fink, X. Wu, P. Y. Kim, A. McGlasson, M. Abdelsamie, T. Emrick, C. M. Sutter-Fella, P. D. Ashby, B. A. Helms, T. P. Russell, *Small* **2023**, e2308560.
[25] a) J. Hu, E. W. C. Spotte-Smith, B. Pan, R. J. Garcia, C. Colosqui, I. P. Herman, *J. Phys. Chem. C* **2020**, *124*, 23949; b) N. Paracini, P. Gutfreund, R. Welbourn, J. F. Gonzalez-Martinez, K. Zhu, Y. Miao, N. Yepuri, T. A. Darwish, C. Garvey, S. Waldie, J. Larsson, M. Wolff, M. Cardenas, *ACS Appl. Mater. Interfaces* **2023**, *15*, 3772; c) H. Li, S. V. Roth, G. Freychet, M. Zhernenkov, N. Asta, L. Wagberg, T. Pettersson, *Biomacromolecules* **2021**, *22*, 4274; d) M. K. Bera, H. Chan, D. F. Moyano, H. Yu, S. Tatur, D. Amoanu, W. Bu, V. M. Rotello, M. Meron, P. Kral, B. Lin, M. L. Schlossman, *Nano Lett.* **2014**, *14*, 6816; e) L. Wu, X. Wang, G. Wang, G. Chen, *Nat. Commun.* **2018**, *9*, 1335.
[26] a) V. Garbin, J. C. Crocker, K. J. Stebe, *J. Colloid Interface Sci.* **2012**, *387*, 1; b) Q. Cheng, H. Fang, R. Cao, Z. Ma, S. Wang, R. Xie, H. Xia, D. Wang, *Supramolecular Materials* **2022**, *1*, 100021; c) M. G. Nikolaides, A. R. Bausch, M. F. Hsu, A. D. Dinsmore, M. P. Brenner, C. Gay, D. A. Weitz, *Nature* **2002**, *420*, 299.
[27] T. Li, A. J. Senesi, B. Lee, *Chem. Rev.* **2016**, *116*, 11128.
[28] J. Forth, P. Y. Kim, G. Xie, X. Liu, B. A. Helms, T. P. Russell, *Adv. Mater.* **2019**, *31*, e1806370.
[29] S. Mhatre, S. Simon, J. Sjoblom, *Anal. Chem.* **2020**, *92*, 12860.
[30] Q. Liu, Z. Sun, J. C. Santamarina, *J. Colloid Interface Sci.* **2021**, *581*, 251.
[31] K. Roger, B. Cabane, *Angew. Chem. Int. Ed. Engl.* **2012**, *51*, 5625.
[32] C. H. Meredith, P. G. Moerman, J. Groenewold, Y. J. Chiu, W. K. Kegel, A. van Blaaderen, L. D. Zarzar, *Nat. Chem.* **2020**, *12*, 1136.
[33] J. Kimling, M. Maier, B. Okenve, V. Kotaidis, H. Ballot, A. Plech, *J. Phys. Chem. B* **2006**, *110*, 15700.

Manuscript received: February 23, 2024
Accepted manuscript online: April 8, 2024
Version of record online: May 3, 2024